# Green Synthesis and Characterization of Iron Nanoparticles Synthesized from Aqueous Extract of *Tabebuia rosea* Family Bignoniacae) and in silico study of ferrous metal iron

**Devika K[1] , Anburaj G [2], Sathish kumar R [3], Manikandan R [4]**

[1,4,] Department of Chemistry, A.V.V.M.S.P College, (Affiliated to Bharathidasan University-Tiruchirappalli), Thanjavur, Tamil Nadu, India

[2]Department of Chemistry PRIST Deemed to be University Thanjavur Tamil Nadu, India

[3,] Department of Botany, Jamal Mohamed College (Autonomous) (Affiliated to Bharathidasan University-Tiruchirappalli), Tamil Nadu, India

**Abstract:**

An aqueous extract of *Tabebuia rosea* has been employed to synthesize iron nanoparticles (FeNPs) by engaging as a reducing agent. IONPs were characterized using UV-spectrophotometer, FTIR, SEM, and EDX Analysis. Fourier transform infrared spectroscopy (FTIR) probed FeNPs exhibited peaks at 2854 and 2926, respectively corresponding to the following C-H stretches, 2850 cm1 (C-H of CH3, CH2, and CH, 2150-2300 cm). A change in color signaled the reaction or the development of dark indicated the existence of FeNPs. By using Blue light analysis, the greatest absorption peak (max) was identified to be at 395 nm. SEM images have been utilized to observe FeNPs with widths spanning 10 and 100 nm. Fe2O3-NPs have shown significant antimicrobial activity against Gram-positive bacteria *B. subtilis*, with a zone of inhibition of 30 mm, However, Gram-negative strains *E. coli* and *P. aeruginosa* with a zone of inhibition of 30 mm and 32 mm respectively. Similarly, Fe2O3-NPs showed substantial good susceptibility towards the tested fungal strain *Aspergillus niger* and *Aspergillus flavus* with the zone of inhibition 14 mm and 20 mm respectively for Fe2O3-NPs compared to 12 mm for fluconazole ($p < 0:05$). Antioxidant activity of various concentrations of IONPs were used (100–500 μg/ml). At the highest concentration (500 μg/ml), IONPs showed a potent DPPH radical scavenging of 89.92%, while standard ascorbic acid showed 91.82% antioxidant activity.

**Keywords**: FeNPs, ***Tabebuia rosea*** UV-Vis, FTIR, XRD, SEM- with EDAX, antimicrobial activity, antioxidant activity.

## Introduction

The claim of nanotechnology in science and know-how to create new nanoscale materials is a swiftly mounting field [1]. Nanotechnology is an exciting research field in this modern science and offering has been a wide variety of products such as nanoparticles, nanorods, and nanotubes of varying dimensions. All these nano-sized products have different specific roles. They vary in size and shape, chemical properties, crystalline, amorphous, and solid states [2]. Various physical science and biological science approaches is the currently used to synthesize metal nanoparticles [3, 4]. The biological synthesis encompasses three steps in which stabilized NPs are synthesized, including the solvent used, an environmentally eco-friendly reducing agent, and a non-toxic capping agent [5]. It is a clear reality that the health hazards of nanoparticle exposure are slowly being understood and need to be addressed quickly [6]. and their production and use are virtually uncontrolled [7]. Numerous physical, chemical, biological, and hybrid methods are now available to synthesize different types of nanoparticles. Green nanotechnology has received a lot of attention and encompasses a variety of processes that reduce or eliminate harmful substances and rejuvenate the environment [8]. Plant extracts typically contain glucose, terpenoids, polyphenols, alkaloids, phenolic acids, and proteins involved in the reduction and stabilization of metal nanoparticles [9]. It has been confirmed that the functional groups, such as –C–O–C–, –C–O–, –C=C–, and –C=O–, present in the phenolic compounds can assist in the formation of metallic nanoparticles [10]. Various types of iron/iron oxides (Fe/FeO/ $FeO_2$ NPs) have been synthesized by using abstracts from plants and other parts such as roots, leaves, fruits, flowers, barks, stems, and seeds. [11],[12],[13]. Plants have developed an array of defense strategies (antioxidant systems) to manage oxidative stress. In these systems, there is a wide variety of antioxidants, which are different in their composition, mechanism, and site of action [14].

## 2. Materials and methods

### 2.1 Plant material and preparation of the extract

Preparation of $H_2O$ extracts. The $H_2O$ extracts were prepared using *TRP* extract. They were collected and washed thoroughly with distilled water to ensure they were free of contamination. Approximately 20 g of fresh bark was weighed and ground using a mortar and pestle. To prepare the plant extract, 20 g of TRP powder was boiled in 100 ml deionized water for 20 min, magnetically stirred at 60 °C, and filtered through filter paper. The extract

was stored in the refrigerator for later use. Approximately 100 g of fresh TRP was collected, thoroughly washed with distilled water, cut into small pieces of plant parts and the *TRP* extract was vacuum-dried. Dried *TRP* (8.3 g) was extracted with 125 ml of DD $H_2O$ and stirred at 60° C. for 30 minutes. The concentrate was allowed to cool before filtering. After extraction, samples were centrifuged at 12000 rpm for 30 minutes. The supernatant was collected, filtered, and stored at -20 °C before use [15].

**2.2. Biosynthesis of Iron Nanoparticles (FeNPs).**

TRP-FeNP was prepared by dissolving FeCl3 in 40 mL of deionized $H_2O$. A 0.1 M $FeCl_3$ solution was prepared. FeNPs were synthesized by mixing a 2:1 volume ratio of 0.1 M $FeCl_3$ solution and aqueous SLE at 60 °C for 30 min with continuous magnetic stirring. A black color appears when $Fe^{+3}$ ions are depleted. Reaction mixtures were prepared in a 2:1 ratio and the maximum UV / visible absorption wavelengths of FeNPs were recorded. BPE-FeNPs were prepared using a 2:1 volume ratio of 0.1 M $FeCl_3$ solution and aqueous BPE (supernatant at ambient temperature). After that, it was shaken by hand for 1 minute and allowed to stand at room temperature for 1 hour. After 10 minutes, the color change of the solution from clear yellow to dark black was observed and recorded. After centrifuging the mixture at 12000 rpm for 30 minutes, the supernatant was poured off. The black paste was redispersed in ethanol to remove any remaining biomolecules before washing with ultrapure water. Centrifugation and redispersion in ethanol and ultrapure water were repeated three times to fully purify the NPs. The light black paste was then oven-dried overnight at 60° C, packed, and stored for characterization [16]

**2.3. Characterization of Biosynthesized Iron Nanoparticles**

**2.3.1. Characterization of FeNPs**

Several methods such as ultraviolet-visible spectroscopy (UV-Vis), Fourier transform infrared spectroscopy (FTIR), scanning electron microscopy, energy dispersive X-ray spectroscopy, X-ray diffraction (XRD), and particle size analyzer Using FeNPs.

**2.3.2. UV-Vis Analysis.**

Changes in the reaction mixture were visually observed and recorded. The samples were then examined spectrophotometrically in the UV-Vis range. The wavelength was scanned from 200 nm to 700 nm at 1 nm intervals.[17]

**2.3.3. FTIR Analysis.**

Measurements were performed using an FTIR system. Extractive functional groups that may have played a role in the synthesis of the iron microstructure were identified using his FTIR scan of iron NPs from *TRP* extract. A transmission mode range of 400–4000 cm-1 was used for the FTIR analysis.[18]

**2.3.4. Scanning electron microscopy (SEM-EDX)**

Scanning electron microscopy (JSM-IT 500, Jeol, Boston, MA, USA), was used to examine the nanoparticles and establish their surface shape.[19] The grain structure was analyzed using SEM equipment (JEOL, USA). Before analysis, the nanoparticles were extensively washed with ethanol to remove any impurities that might have been present.[20] The powdered samples were then dispersed in ethanol using ultrasound, followed by filtration. Samples were finally dried and coated with a (10-15) nm layer of high-purity gold before analysis. Observation by SEM was performed at a fixed electron beam output of 30 kV and a working distance of 11 mm. EDX (energy dispersive X-ray) analysis was performed to confirm the elemental content in the nanoparticles. The samples were analyzed by SEM-EDX at 30 kV and the EDX spectra had an acquisition time of 100 seconds.

**2.3.5. XRD Analysis**.

We used an X-ray diffractometer to study crystalline metallic iron NPs. The instrument used 45 kV Cu-Kα radiation and a monochromatic filter with a wavelength range of 20-80 degrees. The biosynthesized FeNPs were completely dried in powder form before stacking on the XRD apparatus cube.[21]

**2.3.6. Antibacterial Potential.**

The antibacterial activity of living FeNPs from *trp* was tested using the agar diffusion method against two bacterial strains: Bacillus subtilis (MTTC 1133) and Escherichia coli (MTTC 62) from the Microbial Type Culture Collection and Gene Bank ( MTCC). Chandigarh, India, and the zone of inhibition were measured in millimeters using the agar-well diffusion method described in [22]. Antibiotics such as chloramphenicol and gentamicin were used as positive controls in this study.

**2..7 DPPH Radical Scavenging Assay**

The antioxidant assay of FeNPs from *trp* was used against DPPH radical and was determined by UV spectrophotometry at 517 nm. This activity was measured according to the method previously performed [23]. Five different concentrations (100–500 μg/ml) of plant extracts were prepared. Ascorbic acid was used as a standard. 1 ml from each extract and 3 ml of each solvent were mixed with 0.5 ml of 1.0 mM DPPH in methanol and allowed to

react at room temperature for 30 minutes. The same amount of solvent and DPPH to prepare the blank solution which is a control. The sample was prepared in triplicate value for each analysis and the mean value of the absorbance was noted. The DPPH radical scavenging was calculated by the following formula:

DPPH inhibition percentage = [(A0-A1)/A0] x 100

Where, A0 - Absorbance of the control, Al - Absorbance of the FeNP/ascorbic acid.

The inhibitory concentration (IC50) of the plant extract was reported as the number of antioxidants required to reduce the initial DPPH concentration by 50%. A triplicate test was performed and graphs were plotted using the average of three determinations.

## 3 METHODS OF MOLECULAR DOCKING

As an updated version of MIB, MIB2 offers a total of 18 types of metal ions ($Ca^{2+}$, $Cu2^{2+}$,, $Fe^{3+,}$ $Mg^{2+,}$ $Mn^{2+}$, $Zn^{2+}$, $Cd^{2+}$, $Fe^{2+}$, $Ni^{2+}$, $Hg^{2+}$, $Co^{2+}$, $Cu^{2+}$, $Au^{2+}$, $Ba^{2+}$, $Pb^{2+}$, $Pt^{2+}$, $Sm^{3+}$ and $Sr^{2+}$), supportive of binding site predictions. Both prediction systems use the fragment transformation method. (Lu et al., 2022)

## 4. Results and Discussion

### 4.1 UV-VIS spectral analysis

It is widely accepted that UV-Vis spectroscopy can be used to study nanoparticles of controlled size and shape in aqueous suspension. Figure (1) shows the UV-Vis spectrum recorded from the reaction medium after 5 hours. The UV-Vis spectrum of the reaction mixture of $FeCl_3$ solution and Trb extract showed a peak at 266 nm, indicating the presence of FeNPs nanoparticles synthesized by *Tabebuia* rose bark extract shown in figure 1.

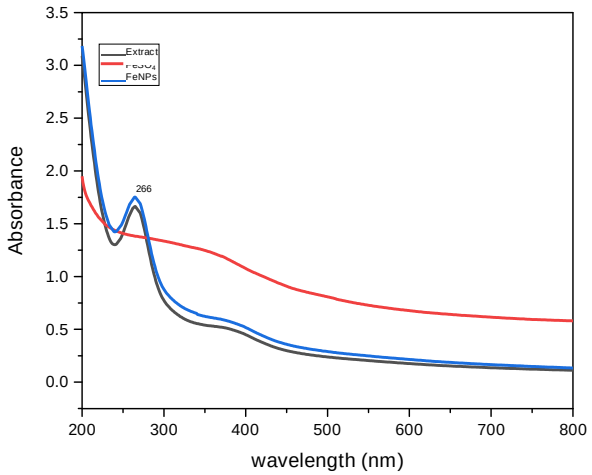


Figure: 1 UV-VIS spectral analysis

The peak increased due to the surface plasmon resonance effects of electrons in the reaction mixture, and peak broadening indicated that the particles were polydisperse. The occurrence of this peak associated with surface plasmons is well documented for a variety of metal nanoparticles ranging in size from 2 nm to 100 nm [17]. UV Spectral Analysis of FeNPs We examined the UV spectra of Fe nanoparticles to identify putative biomolecules involved in the capping and efficient stabilization of Fe nanoparticles synthesized by plant extracts. Peaks were observed for Fe nanoparticles formed by reduction with *Trb* extract (Figure 4.3).

**4.2 FTIR spectral analysis**

The FTIR spectrum (shown Figure: 2 ) bands at 3422 $cm^1$ Bonded N–H/C–H/O–H stretching of amines and amides (O–H stretching vibrations), 2926.27 $cm^1$ (C–H vibration of aliphatic hydrocarbons), FT-IR spectra of Iron oxide nanoparticles and in many of them peaks at 2854 and 2926 which corresponds to C-H stretching is coming,2850 $cm^1$ ( C-H of $CH_3$, $CH_2$, CH), 2150-2300 cm )1 are related to C=N and C " N bonding, respectively.1634.23 cm-1 (C] All spectra present the characteristic bands of the acrylic C = C vibration at 1634 cm-1 and 1555cm-1 asymmetric vibration of Si–O (*1090 cm–1*), 933.04 $cm^1$ C-C Bond, asymmetric vibration of Si–OH .as well as 587cm−1 FTIR peak shows the stretching vibrations due to tetrahedral Fe-O which is referred to Fe–O stretches of iron oxide Comparison of the IR spectrum for ***Trb* extract.** The band at 3422 and 2966 cm−1 corresponds to the OH bond stretching and denotes the aqueous phase, with an increase in the absorption band, indicating the ferric chloride reduction. It is worth mentioning that the same procedures were followed in preparing the extract and synthesized Fe2O3 NP samples concerning the weight used and the sample thickness. The existing findings agree well with the reported values in [24].

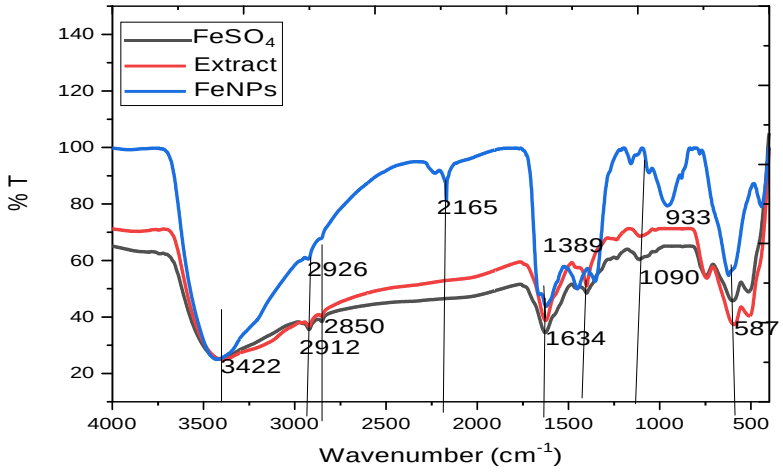


Figure: 2 **FTIR spectral analysis**

### 4.3 Scanning Electron Microscopically (SEM) analysis of AgNPs

SEM analysis (shown Plate-1) was carried out to understand the topology and the size of the Fe-NPs, which showed the synthesis of higher density polydispersed spherical Fe-NPs of various sizes that ranged from 10 to 40nm as well the face-centered cubic structure of the nanoparticles. Most of the nanoparticles aggregated and only a few of them were scattered when observed under SEM (Plate.1). Shows capturing a high-resolution scanning electron microscopic image of single Fe nanoparticles. This variability in size is due to the inability of the secondary metabolites to control the size of the particles formed as compared to chemical synthesis though phytomediated synthesis is a green approach. Since the plant extract contains various secondary metabolites, they act as reducing and stabilizing agents during bio-reduction reactions during the synthesis of metallic nanoparticles [25].

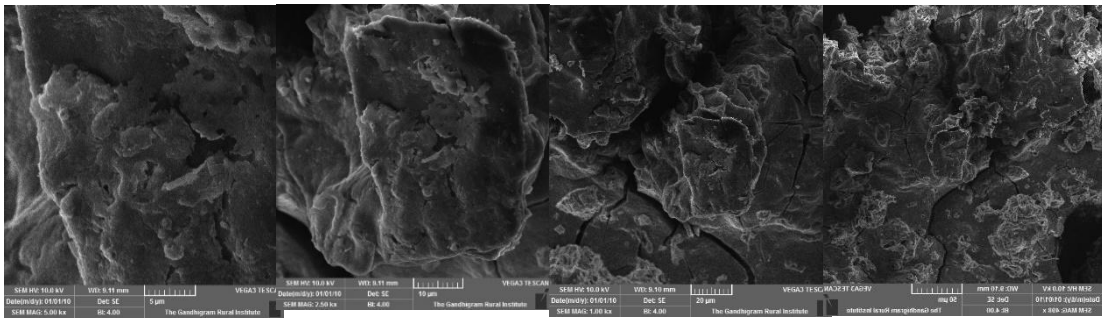

Plate-1 **Scanning Electron Microscopically (SEM) analysis of NPs**

### 4.4 EDAX (Energy Dispersive X-Ray analysis)

**Energy Dispersive X-Ray analysis** is used to predict the elemental composition of constituents. The peak shown from the EDAX field predicts the presence of Fe. It indicates the reduction of fe by isolation compound. Reported that the weight composition of carbon-59.74, Fe-17.19, Ca-4.60, K-1.67, P-0.87, Cl-0.50, and Al-0.12 were 4.98% and 44.78 % respectively (shown in Figure 3). Atomic compositions were high % is Fe and O and also considered as impurities is carbon.

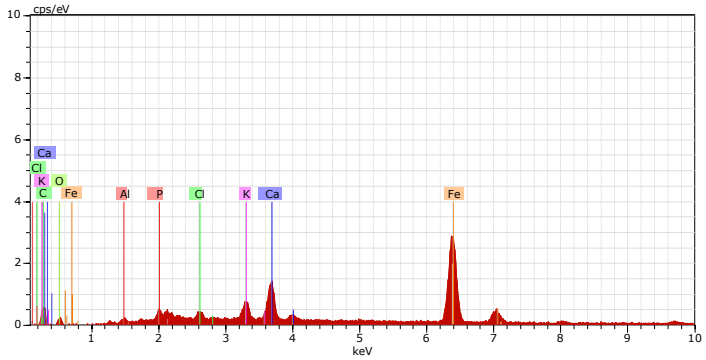


Figure :3 EDAX (Energy Dispersive X-Ray analysis)

Spectrum: sample 9638

El AN Series unn. C norm. C Atom. C Error (1 Sigma)

| El AN Series unn. [wt.%] | C .norm[wt.%] | c.norms wt% | c.atom at.% [at.%] | C.Errorw.t% [wt.%] |
|---|---|---|---|---|
| C-6 | 10.38 | 32.32 | 59.74 | 2.61 |
| Fe- 26 | 13.89 | 43.25 | 17.19 | 0.41 |
| O-8 | 3.54 | 11.03 | 15.3 | 1.23 |
| Ca-20 | 2.67 | 8.3 | 4.6 | 0.12 |
| K-19 | 0.94 | 2.94 | 1.67 | 0.07 |
| P-15 | 0.39 | 1.21 | 0.87 | 0.05 |
| Cl-17 | 0.26 | 0.8 | 0.5 | 0.04 |
| Al- 13 | 0.05 | 0.15 | 0.12 | 0.03 |

### 4.5 X-Ray Diffraction for Ferrous nano particles

The XRD pattern of Fe NPs synthesized from ***trp*** bark XRD is commonly used for determining the chemical composition and crystal structure of a material; therefore, detecting peak. the presence of Fe nanoparticles in plant tissues can be realized by using XRD to

observe the diffraction peaks of the plant. The X-ray diffraction pattern of using biosynthesized FeNPs from the bark extract is shown in (Fig. 4). The crystalline nature of Fe nanoparticles was further confirmed from X-ray diffraction (XRD) analysis showing the XRD pattern of the dried nanoparticles obtained from colloid samples. Several Bragg reflections with 2ø values of 24.934, 37.0359, and 43.8572O indicate the (100), (200), and (300) reflections of metallic silver indicating the cubic crystalline of bioorganic phase that occurs on the surface of the nanoparticle. The observed peak broadening and noise were probably due to macromolecules present in the plant extract which may be responsible for the reduction of Fe ions. Hence XRD pattern thus clearly illustrated that the Fe nanoparticles formed in this present synthesis are crystalline. In addition to the Bragg peaks representative of fcc Fe nanocrystals, additional as yet unassigned peaks are also observed suggesting that the crystallization of the bio-organic phase occurs on the surface of the ferrous nanoparticles. The line broadening of the peaks is primarily due to small particle size. Indexing has been done and data given by XRD.[26]

**4.6 Particle Size Calculation**

(Figure:4 ) From this XRD study, considering the peak at different degrees, average particle size has been estimated by using the Debye-Scherrer formula [27-29]. with the help of the XRD, it gives the miller indices values which indicate the shape of the atoms it may be what type of crystal we can predict the size of the particle so it is very useful to identify.

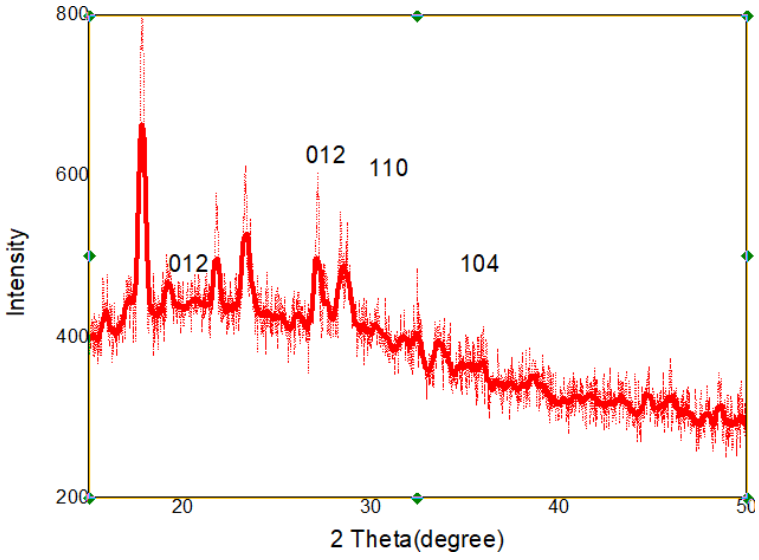


Figure:4 X-Ray Diffraction for Ferrous Nanoparticles

XRD was performed for ferrous nanoparticles, using powder X-ray diffraction shown in Fig 44. There are three diffraction peaks for ferrous were observed 2θ=24°, 30°, 42°

corresponding to (111), (111), (200) this proves the formation of crystalline FeNPs. The pattern of XRD shows the synthesis of ferrous nanoparticles.

**4.7. Antimicrobial Activity of the Synthesized Fe2O3-NPs.**

The antimicrobial susceptibility was tested by agar diffusion method using different concentrations of FeNPs (20 $\mu$L, 40 $\mu$L, 60 $\mu$L, and 80 $\mu$L) The results showed in Figure 5. Compared to the standard ampicillin, Fe2O3-NPs have shown significant antimicrobial activity against Gram-positive bacteria *B. subtilis*, with a zone of inhibition of 30 mm, However, Gram-negative strains *E. coli* and *P. aeruginosa* with the zone of inhibition of 30 mm and 32 mm respectively. Similarly, Fe2O3-NPs showed significant good susceptibility towards the tested fungal strain *Aspergillus niger* and *Aspergillus flavus* (Figure:6) in comparison to the standard fluconazole, and the zone of inhibition was 14 mm and 20 mm respectively for Fe2O3-NPs compared to 12 mm for fluconazole ($p < 0:05$).

The antimicrobial activity of Fe2O3-NPs synthesized by the *M. ornate* flower sheath has been tested activity against *S. aureus* and *S. agalactiae* [30].

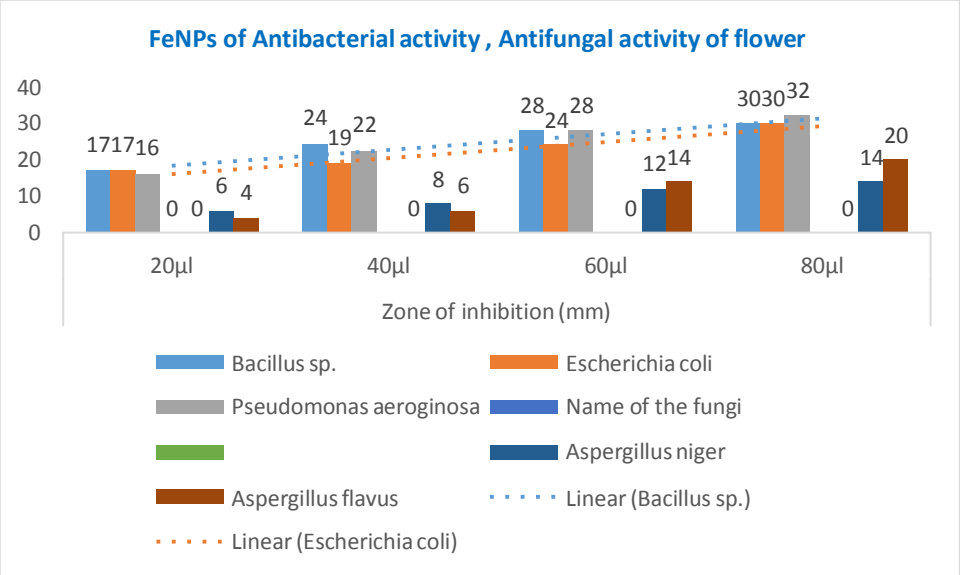


Figure:5 Antibacterial activity of FeNPs and Antifungal activity of FeNPs

| **FeNPs of Antibacterial activity, Antifungal activity** | | | | |
|---|---|---|---|---|
| **Name the bacteria** | **Zone of inhibition (mm)** | | | |
| | **20µl** | **40µl** | **60µl** | **80µl** |
| *Bacillus* sp. | 17 | 24 | 28 | 30 |

| | | | | |
|---|---|---|---|---|
| *Escherichia coli* | 17 | 19 | 24 | 30 |
| *Pseudomonas aerogino* | 16 | 22 | 28 | 32 |
| **Name of the fungi** | Zone of the inhibition (mm) | | | |
| | 20µl | 40µl | 60µl | 80µl |
| *Aspergillus niger* | 6 | 8 | 12 | 14 |
| *Aspergillus flavus* | 4 | 6 | 14 | 20 |

**4.9 DPPH radical scavenging activity**

1,1- Diphenyl-2-picrylhydrazyl radical is a commonly used method to assess the free radical scavenging ability of various extracts and compounds. DPPH is a nitrogen-centered radical and the changes of color from violet to yellow upon reduction are observed by the process of hydrogen or electron donation. If the test extract could perform this reaction antioxidant potential can be measured of the same free radical scavenging activity of the test extract is assessed. It was observed that the free radical scavenging activities of trb increased with increasing concentration. [31].

The $IC_{50}$ value was used to calculate the antioxidant activity. The $IC_{50}$ value shows the antioxidant concentration required to reduce free radicals by 50%. The lower the $IC_{50}$, the better the scavenging activity of antioxidant samples. Figure 7 shows the antioxidant activity of various concentrations of IONPs (100–500 µg/ml). At the highest concentration (500 µg/ml), IONPs showed a potent DPPH radical scavenging of 89.92%, while standard ascorbic acid showed 91.82% antioxidant activity. Previous studies supported that IONPs have excellent antioxidant activities [32] Therefore, it proposed that IONPs scavenge free radicals by transferring hydrogen atoms or donating electrons to DPPH radicals.

| **Concentrations (µg/ml)** | **% of inhibitions** | |
|---|---|---|
| | **Flower FeNPs** | **Standard as Ascorbic acid** |
| 100 | 21.14 | 24.12 |
| 200 | 34.36 | 40.46 |
| 300 | 59.12 | 61.37 |
| 400 | 75.79 | 80.55 |
| 500 | 89.92 | 91.82 |
| $IC_{50}$ Value | 308.97 | 245 |

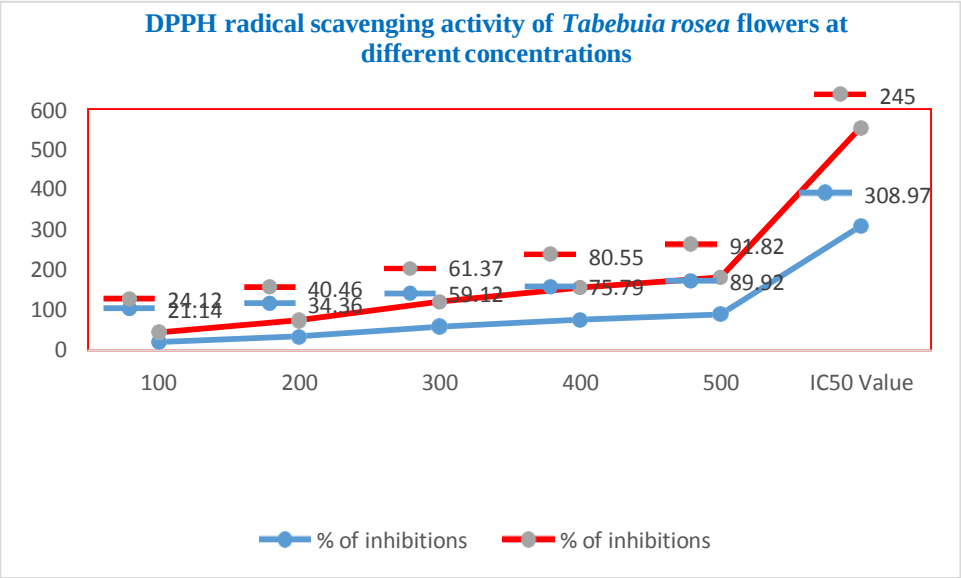


Values are expressed as Mean± SD for triplicates

Figure:7 DPPH radical scavenging activity

**4.10 Alpha-amylase / glucosidase Frequency of amino acid and Fe $^{3+}$ & Fe$^{2+}$ binding affinity**

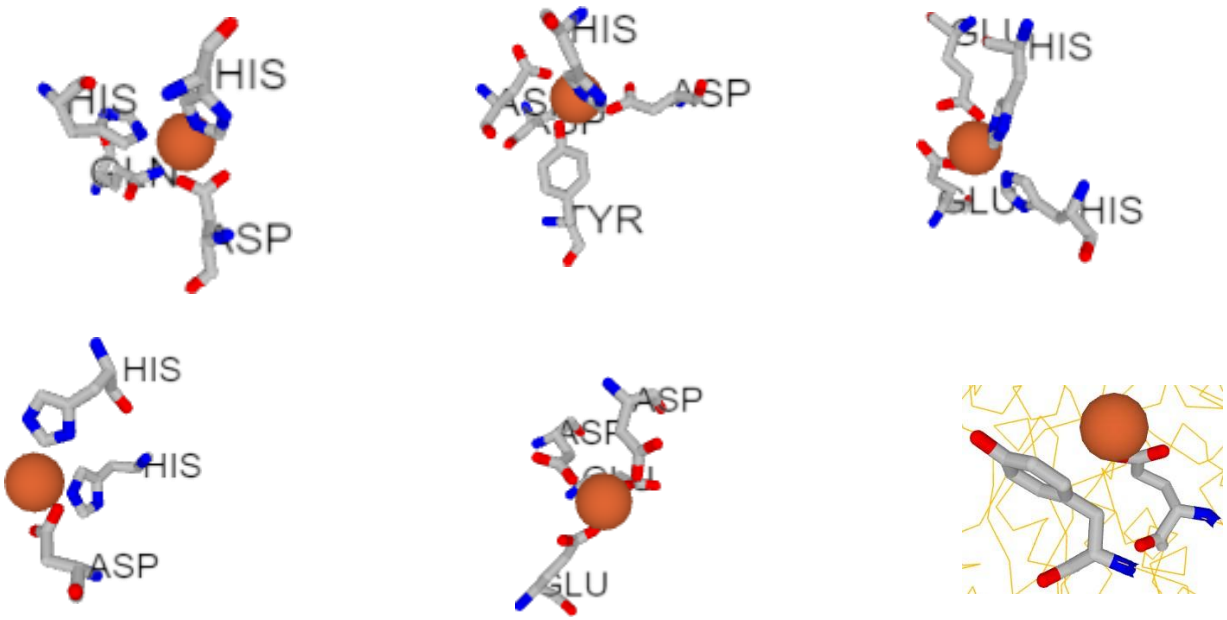


| H-Histidine | D-aspartic acid | E-glutamic acid | L-leucine | S-serine | R-arginine | A-alanine | Q-glutamine | P-proline |
|---|---|---|---|---|---|---|---|---|
| 16 | 17 | 17 | 4 | 4 | 3 | 1 | 3 | 0 |
| 30 | 19 | 12 | 2 | 4 | 6 | 1 | 4 | 1 |

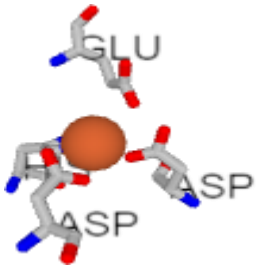


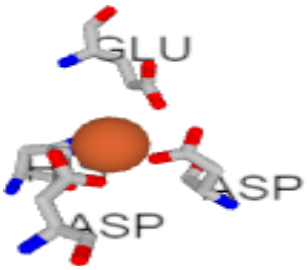


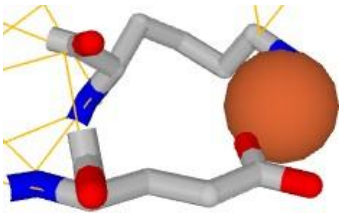

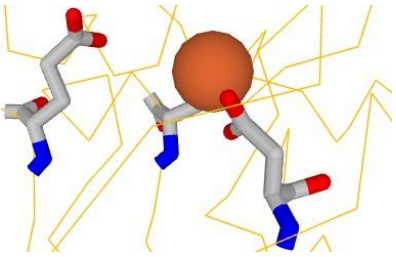

| H-Histidine | D-aspartic acid | E-glutamic acid | L-leucine | S-serine | R-arginine | A-alanine | Q-glutamine | P-proline |
|---|---|---|---|---|---|---|---|---|
| 51 | 30 | 17 | 4 | 13 | 6 | 10 | 3 | 2 |
| 12 | 16 | 5 | 1 | 13 | 5 | 0 | 1 | 0 |

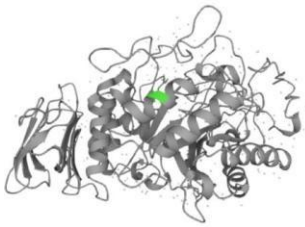

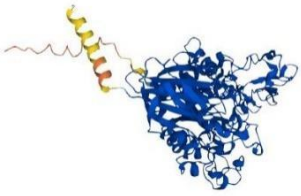

**alpha-amylase- P56634 Q95WY5**

**alpha-glucosidase**

A performance comparison between MIB and MIB2 MIB2 benefits from more protein structures becoming available since the development of MIB. For each type of metal ion, the numbers of binding templates in MIB2 range from 1.24 to 10.72 times the numbers in MIB. (31) The propensity of various protein and atom types on binding A greater likelihood of type 2 diabetes is linked to excess iron preservation and may harm pancreatic -cells and promote resistance to insulin via enhanced oxidative stress 22. The primary method of storing iron in the body is ferritin, which is a crucial protein that controls iron homeostasis. (Liu et al., 2020) In general, the molecular docking tests provided insight into the divided molecules' possible inhibiting the enzyme alpha and potential methods for the structure-based design or enhancement of such compounds or novel compounds. (Etsassala et al., 2022) This result is showing the many amino acids and is also given in table (

)high binding energy is histidine Fe2+(51) lowest binding is 2, and Fe3+ binding energy is 12 (H-Histidine) lowest binding energy 5 list H-Histidine, D-aspartic acid, E-glutamic acid, L-leucine, S-serine, R-arginine, A-alanine, Q-glutamine, P-proline alpha amylase-en P56634(Enzymes are protein), alpha-glucosidase Q95WY5(Enzymes are protein) this protein is more active with Fe2+ so finally we try to clinical work then confirmed.

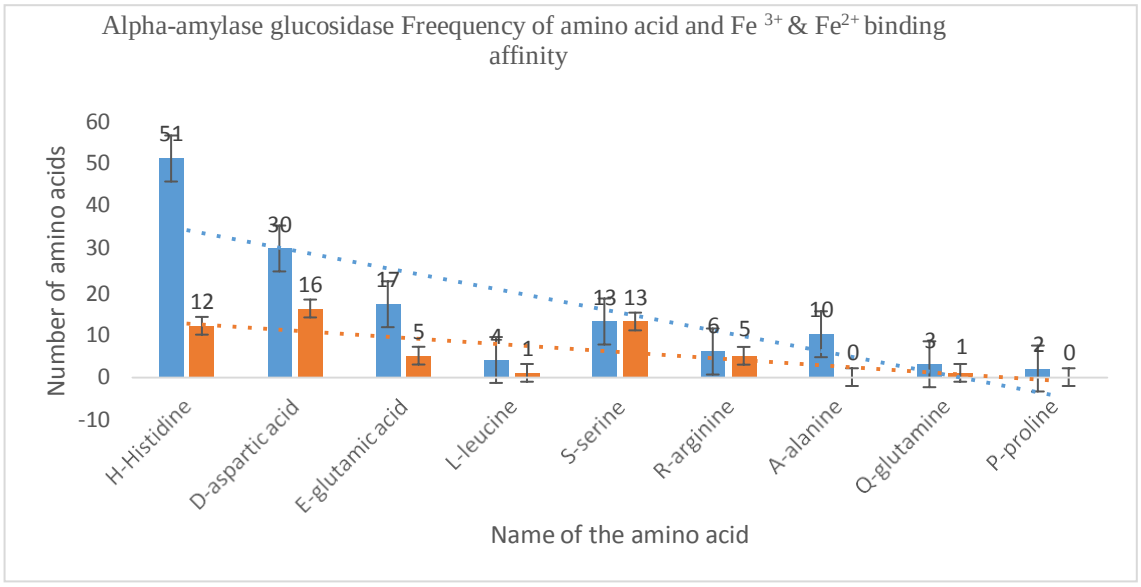


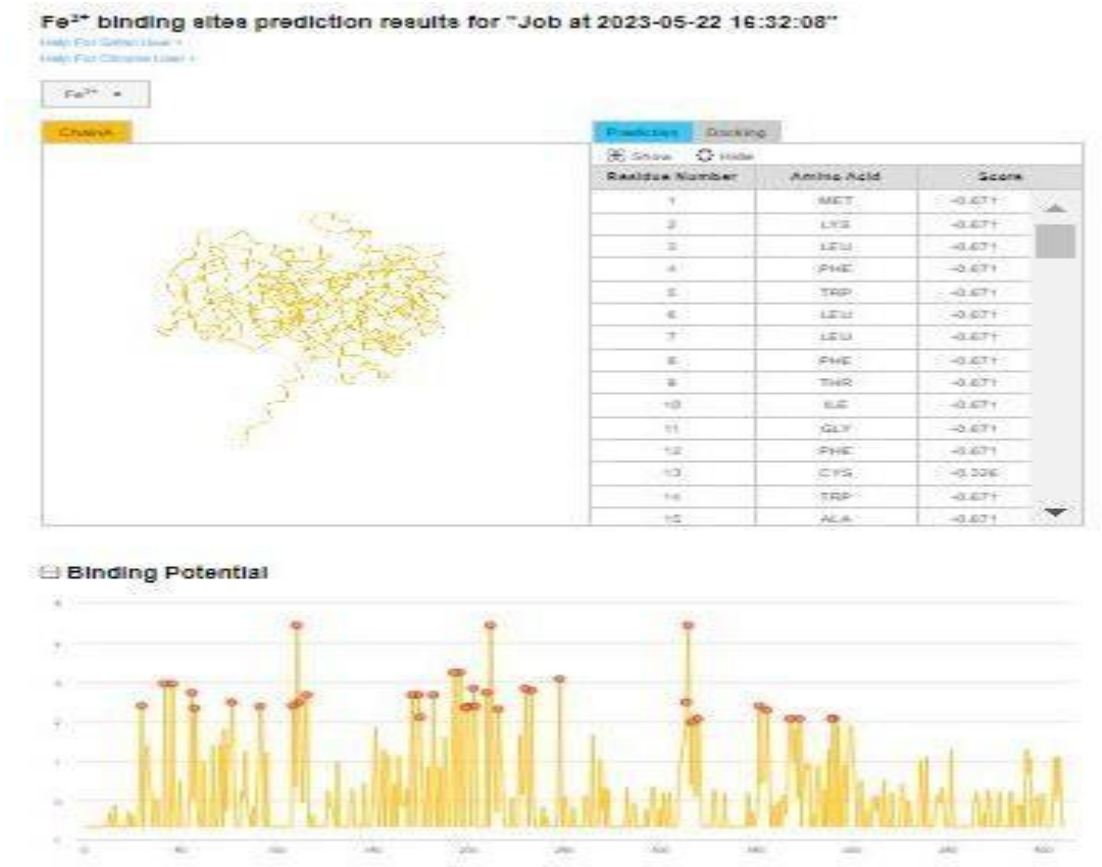

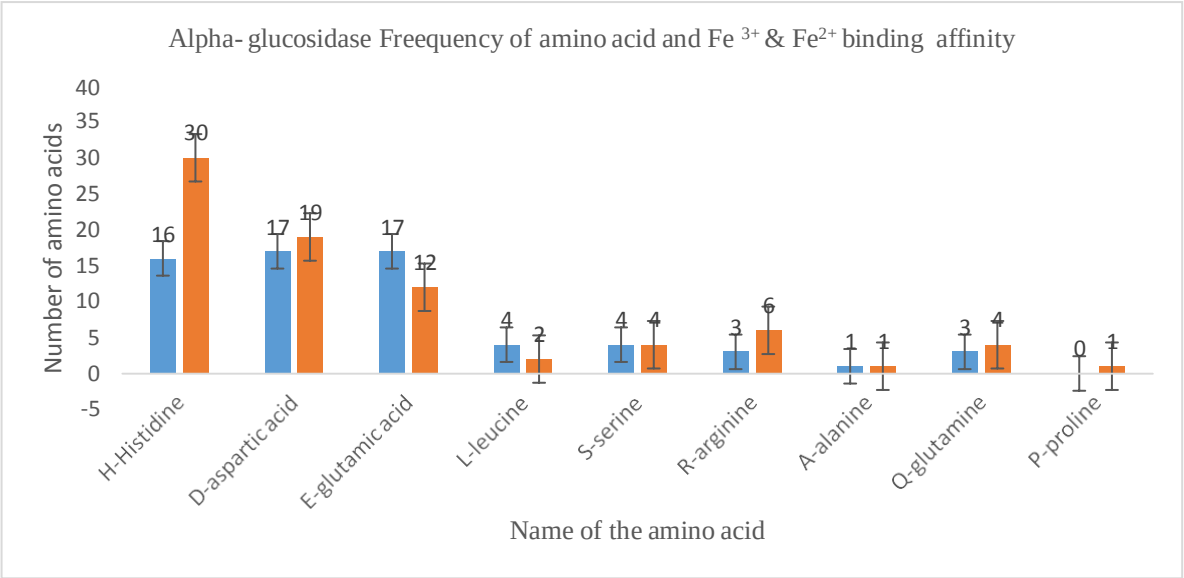


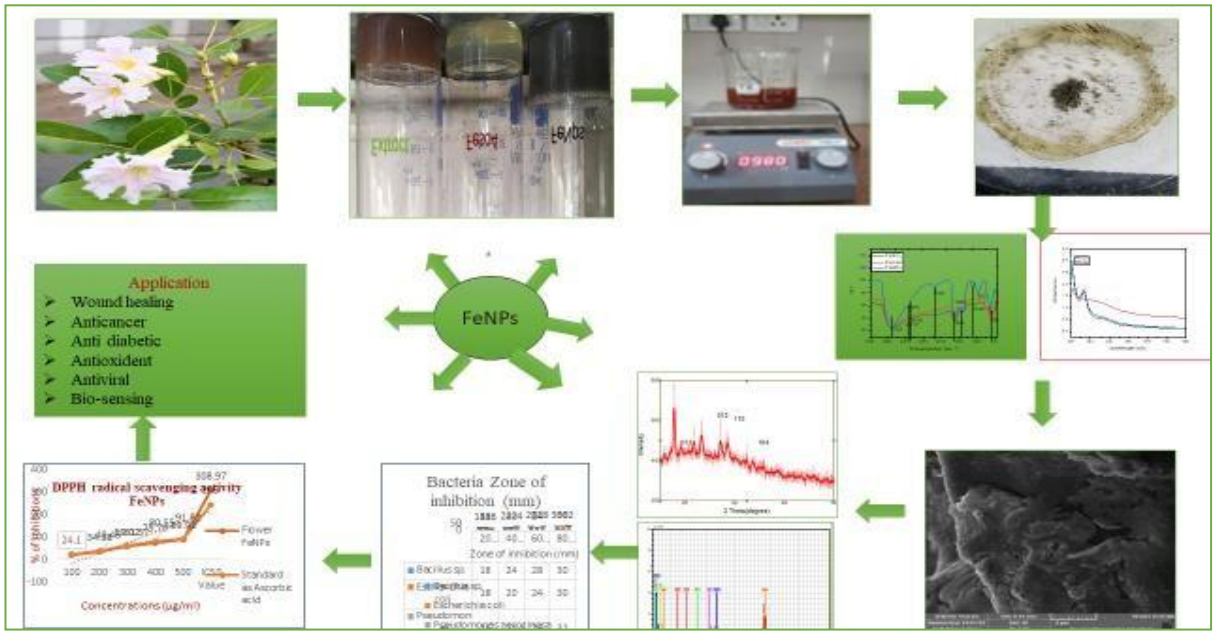


Figure:7 Graphical Abstract for FeNPs

## 5. Conclusions

From this *trp* was used to magnificently synthesize iron nanoparticles. The biomolecules in bark extracts were involved in FeNP formation and stability. UV-visible spectroscopy, SEM, XRD, and EDX were used to characterize the size, morphology, crystal structure, and stability. Iron nanoparticles have potent antioxidant, and cytotoxic, properties. Overall, FeNPs exhibit considerable antibacterial potency and can be used as antibacterial agents against pathogenic bacteria while remaining non-toxic to humans, and did antioxidant also. Future studies are needed to identify the mechanisms involved in the synthesis of FeNPs by *trb* and their biomedical applications.

**Data Availability**

The data used to support the findings of this study are available from the corresponding author upon request.

**Conflicts of Interest**

The authors declare that they have no conflicts of interest.

**Acknowledgments:**

We express our gratitude to the management of A.V.V.M. Sri Pushpam College (Autonomous), Poondi, for providing us with the necessary support and research facilities to complete this work.

**6.References**

1) Albrecht, M.A.; Evans, C.W.; Raston, C.L. Green Chemistry and the Health Implications of Nanoparticles. Green Chem. 2006, 8, 417. [CrossRef]
2) Alvi, G. B. et al. Biogenic selenium nanoparticles (SeNPs) from citrus fruit have anti-bacterial activities. Sci. Rep. 11, 1–11 (2021).
3) S. O'Brien, L. Brus, and C. B. Murray, “Synthesis of monodisperse nanoparticles of barium titanate: toward a generalized strategy of oxide nanoparticle synthesis,” Journal of the American Chemical Society, vol. 123, no. 48, pp. 12085-12086, 2001.
4) G. A. Naeem, "Green synthesis of gold nanoparticles from Coprinus comatus, Agaricaceae, and the effect of ultraviolet irradiation on their characteristics," Walailak Journal of Science and Technology, vol. 18, no. 8, 2021.
5) J. K. Patra and K. H. Baek, “Green nanobiotechnology: factors affecting synthesis and characterization techniques,” Journal of Nanomaterials, vol. 2014, 12 pages, 2014.
6) Kandlikar, M., Ramachandran, G., Maynard, A., Murdock, B., & Toscano, W. A. (2007). Health risk assessment for nanoparticles: A case for using expert judgment. Journal of Nanoparticle Research, 9, 137-156.10.1007/s11051-006-9154-x.

7) Wardak A, Gorman ME, Swami N, Rejeski D. Environmental regulation of nanotechnology and the TSCA. IEEE Technol Soc Mag. 2007;26:48–56. 10.1109/MTAS.2007.4295056.Search in Google Scholar

8) S. Kanagasubbulakshmi, K. Kadirvelu. Green Synthesis of Iron Oxide Nanoparticles using Lagenaria Siceraria and Evaluation of its Antimicrobial Activity Defence Life Science Journal. 2017; 2(4): 422-427.

9) T. Shahwana, S. Abu Sirriaha, M. Nairata, et al., "Green synthesis of iron nanoparticles and their application as a Fenton-like catalyst for the degradation of aqueous cationic and anionic dyes," Chemical Engineering Journal, vol. 172, pp. 258–266, 2011.

10) P. Salgado, K. Márquez, O. Rubilar, D. Contreras, and G. Vidal, "The effect of phenolic compounds on the green synthesis of iron nanoparticles (FexOy-NPs) with photocatalytic activity," Applied Nanoscience, vol. 9, pp. 371–385, 2019.

11) B. Kumar, K. Smita, S. Galeas, et al., "Characterization and application of biosynthesized iron oxide nanoparticles using citrus paradise peel: a sustainable approach," Inorganic Chemistry Communications, vol. 119, Article ID 108116, 2020.

12) P. N. V. K. Pallelaa, S. Ummey, L. K. Ruddaraju, et al., "Antibacterial efficacy of green synthesized α-Fe2O3 nanoparticles using Sida cordifolia plant extract," Heliyon, vol. 5, Article ID e02765, 2109.

13) Šutka, M. Vanags, A. Spule, et al., "Identifying iron-bearings nanoparticles precursor for thermal transformation into the highly active hematite photo-Fenton catalyst," Catalyst, vol. 10, p. 778, 2020.

14) R Sathish Kumar, G Anburaj, A Subramanian, S Vasantha, and A Panneer Selvam. In vitro antioxidant potential of leaf extracts of Capparis zeylanica Linn. The Pharma Innovation Journal 2019; 8(4): 176-181.

15) E. C. Njagi, H. Huang, L. Stafford, et al., "Biosynthesis of iron and silver nanoparticles at room temperature using aqueous sorghum bran extracts," Langmuir, vol. 27, no. 1, pp. 264–271, 2011.

16) Yosmery Vitta a,⇑, Maice Figueroa a , María Calderon b , Carlos Ciangherotti. Synthesis of iron nanoparticles from aqueous extract of Eucalyptus robusta Sm and evaluation of an antioxidant and antimicrobial activity. Materials Science for Energy Technologies 3 (2020) 97–103.

17) Ting, A. S. Y., & Chin, J. E. (2020). Biogenic synthesis of iron nanoparticles from apple peel extracts for decolorization of malachite green dye. Water, Air, & Soil Pollution, 231(6), 278.

18) Hassan Al-Karagoly*, Atiaf Rhyaf, Hala Naji, Salim Albukhaty, Faizah A. AlMalki, Amal A. Alyamani, Jawaher Albaqami, and Salman Aloufi. Green synthesis, characterization, cytotoxicity, and antimicrobial activity of iron oxide nanoparticles using Nigella sativa seed extract. Green Processing and Synthesis 2022; 11: 254–265.

19) 15.d.Nahari, M.H.; Al Ali, A.; Asiri, A.; Mahnashi, M.H.; Shaikh, I.A.; Shettar, A.K.; Hoskeri, J. Green Synthesis and Characterization of Iron Nanoparticles Synthesized from Aqueous Leaf Extract of Vitex leucoxylon and Its Biomedical Applications. Nanomaterials 2022, 12, 2404. https://doi.org/10.3390/ nano12142404.

20) 15.e. TheintTheint Win1,2, Sikandar Khan3, Bo Bo2, Shah Zada4 & PengCheng Fu1. Green synthesis and characterization of Fe3O4 nanoparticles using Chlorella-K01 extract for potential enhancement of plant growth stimulating and antifungal activity. Scientifc Reports | (2021) 11:21996 | https://doi.org/10.1038/s41598-021-01538-2.

21) Thiyagarajan, M., & Suriyavathana, M. (2010). Phytochemical and antimicrobial screening of Manihot escalate Crantz varieties Mulluvadi I, CO3 root bark. International Journal of Biotechnology and Biochemistry, 6(6), 859-864.

22) Sathish Kumar R, Anburaj G, Mageshkumar R, Subramanian A, Vasantha S. In vitro assessment of antioxidant and anticancer activities of Capparis zeylanica L. leaf extracts against human breast cancer (MCF-7). International Journal of Botany Studies. 6(6)1301-1305 (2021).

23) Henglein, (1993). Physicochemical properties of small metal particles in solution:" microelectrode" reactions, chemisorption, composite metal particles, and the atom-to-metal transition. The Journal of Physical Chemistry, 97(21), 5457-5471

24) A. F. Buarki, 1 H. AbuHassan, 1 F. Al Hannan , 2 and F. Z. Henari. Green Synthesis of Iron Oxide Nanoparticles Using Hibiscus rosa sinensis Flowers and Their Antibacterial Activity. Hindawi Journal of Nanotechnology Volume 2022, Article ID 5474645, 6 pages https://doi.org/10.1155/2022/5474645.

25) 17.B. Edwin Shigwenya Madivoli1 · Patrick Gachoki Kareru1 · Ernest Gachui Maina1 · Augustine Otieno Nyabola1 · Sammy Indire Wanakai1 · Jared Onyango Nyang'au1,2. Biosynthesis of iron nanoparticles using Ageratum conyzoides extracts their antimicrobial and photocatalytic activity. SN Applied Sciences (2019) 1:500 | https://doi.org/10.1007/s42452-019-0511-7

26) Sun, W., Li, N., & He, S. (2002). Large- scale morphological survey of mouse retinal ganglion cells. Journal of Comparative Neurology, 451(2), 115-126.

27) Nath, P., & Perez, P. F. (2007). Proton stability in grand unified theories, in strings, and branes. Physics Reports 441(5-6), 191-317.

28) Nath, A., Dixit, M., Bandiya, A., Chavda, S., & Desai, A. J. (2008). Enhanced PHB production and scale-up studies using cheese whey in fed-batch culture of Methylobacterium sp. ZP24. Bioresource Technology, 99(13), 5749-5755.

29) Bykkam, S., Ahmadipour, M., Narisngam, S., Kalagadda, V. R., & Chidurala, S. C. (2015). Extensive studies on X-ray diffraction of green synthesized silver nanoparticles. Adv. Nanopart, 4(1), 1-10.

30) .A S. Saranya, K. Vijayarani, and S. Pavithra, "Green synthesis of iron nanoparticles using aqueous extract of Musa ornata flower sheath against pathogenic bacteria," Indian Journal of Pharmaceutical Sciences, vol. 79, no. 5, pp. 688–694, 2017

31) Nuutila, A. M., Puupponen-Pimiä, R., Aarni, M., & Oksman-Caldentey, K. M. (2003). Comparison of antioxidant activities of onion and garlic extracts by inhibition of lipid peroxidation and radical scavenging activity. Food Chemistry, 81(4), 485-493.

32) Norul Aini Zakariya, Shahnaz Majeed, Wan Hafizah W. Jusof. Investigation of antioxidant and antibacterial activity of iron oxide nanoparticles (IONPS) synthesized from the aqueous extract of Penicillium spp. Sensors International 3 (2022) 100164

33) Etsassala, N. G. E. R., Badmus, J. A., Marnewick, J. L., Iwuoha, E. I., Nchu, F., Hussein, A. A., & Egieyeh, S. (2022). Alpha-Glucosidase and Alpha-Amylase Inhibitory Activities, Molecular Docking, and Antioxidant Capacities of Plectranthus colonic Constituents. Antioxidants, 11(2), 1–12. https://doi.org/10.3390/antiox11020378

34) Liu, J., Li, Q., Yang, Y., & Ma, L. (2020). Iron metabolism and type 2 diabetes mellitus: A meta-analysis and systematic review. Journal of Diabetes Investigation, 11(4), 946–955. https://doi.org/10.1111/jdi.13216

35) Lu, C. H., Chen, C. C., Yu, C. S., Liu, Y. Y., Liu, J. J., Wei, S. T., & Lin, Y. F. (2022). MIB2: metal ion-binding site prediction and modeling server. Bioinformatics (Oxford, England), 38(18), 4428–4429. https://doi.org/10.1093/bioinformatics/btac534